Characteristics of aeration in the flow downstream of a radial gate with a sudden fall-expansion aerator in a discharge tunnel

Shuai Li, Jianmin Zhang, Xiaoqing Chen, Gordon G. D. Zhou and Jiangang Chen

ABSTRACT

The mechanisms of cavitation damage in flood releasing tunnels remain unclear. In this study a series of physical experiments and numerical calculations were conducted to investigate the flow pattern, pressure distribution and cavitation downstream of a sudden fall-expansion aerator in a discharge tunnel. When the radial gate was partly open, the bottom cavity length reduced drastically, the lateral cavity disappeared, and the flow cavitation index near the sidewalls was less than 0.2. The pressure on the floor and sidewalls can be divided into four regimes: the cavity regime, the impact regime, the reflective regime and the stable regime. The time-average pressure is subject to a unimodal distribution when the gate is fully open, whereas a bimodal distribution is presented when the gate is partly open. The negative pressure regime presented an elliptic shape. Cavitation erosion occurred easily on lateral expansion sidewalls in the tunnel with the radial gate partly open.

Key words | discharge tunnel, numerical model, physical experiments, radial gate opening, sudden fall-expansion aerator

Shuai Li
Xiaoqing Chen
Gordon G. D. Zhou
Jiangang Chen
Key Laboratory of Mountain Hazards and Earth Surface Process/Institute of Mountain Hazards and Environment, Chinese Academy of Sciences and Ministry of Water Conservancy,
Chengdu 610041,
China

Jianmin Zhang (corresponding author)
State Key Laboratory of Hydraulics and Mountain River Engineering,
Sichuan University,
Chengdu 610065,
China
E-mail: *zhangjianmin@scu.edu.cn*

INTRODUCTION

Aerators and radial gates with sudden fall-expansion facilities were often adopted to eliminate cavitation erosion in flood releasing tunnels of hydropower engineering (Pfister *et al.* 2001; Pfister & Hager 2010; Wu & Ma 2013; Hager & Boes 2014). Unfortunately, cavitation damage still occurred in some prototype projects. The performance of cavitation erosion is largely governed by hydraulic characteristics and operational factors. It is therefore important that the flow properties and gate operation are sufficiently researched.

There is considerable research on cavitation in discharge engineering. Nie *et al.* (2006) revealed that the dominant factor governing the cavitation on sidewalls is low pressure. The critical conditions of air concentration and flow velocity to prevent cavitation erosion were proposed by Dong & Su (2006). The results showed that the pressure increased remarkably in the cavitation region because of aeration. Variations of pressure and cavitation with air concentration, pressure waveforms and the cavitation erosion level of types of concrete were obtained by Dong *et al.* (2007). The air concentration, pressure and velocity along the jet formed by a bottom aerator were studied by Arantes *et al.* (2010). Zhang *et al.* (2010) considered that the low pressure and insufficient aeration on the sidewalls were mainly due to the operation of the gate. However, the intrinsic cause of cavitation erosion is still not clear. Air-water flow properties in a curve-connective discharging tunnel were investigated by Li *et al.* (2016a). The results indicated that the sidewalls can be protected against cavitation by installing cross-section aerators.

doi: 10.2166/ws.2017.155

Nowadays, numerical models are used frequently as they enable less time and money to be spent. The Reynolds-averaged Navier–Stokes equations and $k-\varepsilon$ model were used to simulate the air-water flow in stilling basins (Chen *et al.* 2010), the turbulent flow in steep open channels (Aghebatie & Hosseini 2016) and the free surface of the flow in chutes (Bazargan & Aghebatie 2015). A good agreement was found between the numerical results and experimental data. The hydraulic characteristics along the sidewall downstream of a sudden lateral enlargement and vertical drop aerator are simulated by Li *et al.* (2011). It is shown that this type of aerator can prevent cavitation damage of the sidewall. Empirical formulae were presented to calculate the pressure and cavitation index on sidewalls downstream of a radial sluice by combining a realizable $k-\varepsilon$ turbulent model with a mixture multiphase model (Li *et al.* 2016b).

The mechanism of cavitation erosion on sidewalls in tunnels is not well understood. Few researchers have systematically investigated the flow behavior downstream of a radial gate with a sudden fall-expansion aerator in a tunnel. In order to evaluate the flow characteristics of a discharging tunnel in Zipingpu dam, a series of experiments and numerical simulations (combining the realizable $k-\varepsilon$ turbulence model with a mixture multiphase flow model) were conducted to investigate the flow pattern, pressure distribution and flow cavitation index on both the floor and sidewalls. This research provides a new understanding for simulating air-water flow in tunnels, and optimizing the design of sidewalls downstream of a radial gate with a sudden fall-expansion aerator and the operation of the gate.

Experimental set-up

The physical model was combined with a real world case of a tunnel in Zipingpu dam, located in China. The model (length: 18 m, height: 6.4 m) consists of a water tank, inlet section, test region, tail-water region, backwater channel, weir and underground water reservoir (Figure 1). The sudden fall-expansion aerator is installed at the end of the radial gate. The tunnel (slope $i = 0.025$) is divided into three regimes: the first regime (length: 9.7 m, identical width: 3.8 m); the second regime with diffuser angle of 2.23° (length: 15 m); and the third regime (length: 6.3 m, identical width: 5.0 m). There are two columns of test points arranged on the right wall downstream of the chamber. The test region of the flume was fabricated with glass sides so as to observe the flow pattern. Air concentration and velocity were recorded using a CQY-Z8a instrument (Bai *et al.* 2016). Piezometers were installed to measure the pressure.

Scale effects exist in the physical model. In the similarity laws, the Froude number, Reynolds number, Weber number and cavitation index should all satisfy their criteria. However, it is very difficult to achieve complete similarity between the prototype and its model. In general, the main methods to reduce scale effects include: (1) ensure the Reynolds number is large than 1×10^6 to meet the fully developed turbulent flow; (2) use a large scale model; (3) install a control system of gas nuclear content in cavitation model devices. Heller (2011) proposed that a typical hydraulic model scale to investigate cavitation is 1:10 to 1:30. The present scale is 1:25, so the scale effects may therefore not necessarily be

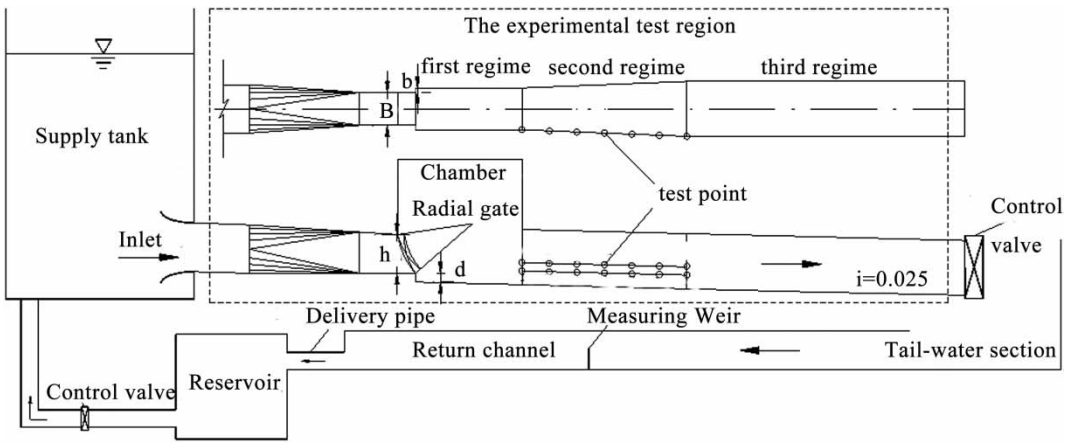

Figure 1 | Schematic diagram of test model.

negligible. In addition, the experimental Reynolds numbers ranged from 6.8×10^6 to 33×10^6.

Numerical model (governing equations and turbulence closure model)

Three-dimensional Reynolds-averaged continuity and momentum equations were used to simulate the air-water flow. For an incompressible, Newtonian fluid flow, these equations can be expressed as:

$$\frac{\partial \rho_m}{\partial t}+\nabla(\rho_m \vec{v}_m)=0 \tag{1}$$

$$\frac{\partial}{\partial t}\rho_m \vec{v}_m+\nabla\cdot(\rho_m \vec{v}_m \vec{v}_m)=-\nabla p_m+\nabla\cdot(\mu_{eff}\nabla \vec{v}_m)+\rho_m g + \nabla\cdot\left(\sum_{k=1}^{n}\alpha_k\mu_{eff}\nabla \vec{v}_k-\sum_{k=1}^{n}\alpha_k\rho_k \vec{v}_{dr,k}\vec{v}_{dr,k}\right) \tag{2}$$

where ρ_m, $\vec{v}_m$ and p_m are the mixture density, velocity and pressure, respectively; t is the solution time; μ_{eff} is the effective viscosity; g is the acceleration of gravity; α_k, ρ_k, and $\vec{v}_k$ are the volume fraction, density and velocity of the k-phase, respectively; $\vec{v}_{dr,k}$ is the diffusion velocity.

The Reynolds stress term is modeled using the realizable $k-\varepsilon$ turbulence model (Shih *et al.* 1995). The transport equations for the turbulent kinetic energy (k) and its dissipation rate (ε) are as follows:

$$\frac{\partial}{\partial t}(\rho k)+\frac{\partial}{\partial x_i}(\rho \vec{v}_i k)=\frac{\partial}{\partial x_j}\left[\left(\mu+\frac{\mu_t}{\sigma_k}\right)\frac{\partial k}{\partial x_j}\right]+G_k-\rho\varepsilon \tag{3}$$

$$\frac{\partial}{\partial t}(\rho \varepsilon)+\frac{\partial}{\partial x_i}(\rho \vec{v}_i \varepsilon)=\frac{\partial}{\partial x_j}\left[\left(\mu+\frac{\mu_t}{\sigma_\varepsilon}\right)\frac{\partial \varepsilon}{\partial x_j}\right]+\rho c_1 S\varepsilon - \rho c_2\frac{\varepsilon^2}{k+\sqrt{v\varepsilon}} \tag{4}$$

where ρ is the fluid density; x_i ($i=1, 2, 3$) are the coordinates in the Cartesian coordinate system; $\vec{v}_i$ ($i=1, 2, 3$) are the velocity components; c_1 and c_2 are empirical constants; v is the turbulent viscosity; G_k represents the generation of turbulence kinetic energy due to the mean velocity gradients; and μ is the fluid viscosity. Closure coefficients and auxiliary relations (for incompressible flow) are as follows:

$$\left.\begin{aligned}&\sigma_k=1.0,\ \sigma_\varepsilon=1.2,\ c_2=1.9,\ G_k=\left(\frac{\partial v_j}{\partial x_i}+\frac{\partial v_i}{\partial x_j}\right)\frac{\partial v_i}{\partial x_j},\ c_1=\max\left[0.43,\ \frac{\eta}{\eta+5}\right]\\&\eta=\frac{Sk}{\varepsilon},\ S=\sqrt{2S_{ij}S_{ij}},\ S_{ij}=\frac{1}{2}\left(\frac{\partial v_j}{\partial x_i}+\frac{\partial v_i}{\partial x_j}\right),\ \mu_t=\rho C_\mu\frac{k^2}{\varepsilon},\ \varphi=\frac{1}{3}\arccos(\sqrt{6}W),\ W=\frac{S_{ij}S_{jk}S_{ki}}{\sqrt{2S_{ij}S_{ij}}}\end{aligned}\right\} \tag{5}$$

Instead of a constant, C_μ is a function of the mean strain and rotation rates as shown in Equation (6):

$$C_\mu=\frac{1}{A_0+A_s(U^*k/\varepsilon)} \tag{6}$$

where $U^*=\sqrt{S_{ij}S_{ij}+\tilde{\Omega}_{ij}\tilde{\Omega}_{ij}}$, $\tilde{\Omega}_{ij}=\Omega_{ij}-2\varepsilon_{ijk}\omega_k$, $\Omega_{ij}=\bar{\Omega}_{ij}-\varepsilon_{ijk}\omega_k$, $\tilde{\Omega}_{ij}$ is the mean rate of rotation tensor in a rotating reference frame with the angular velocity ω_k; S_{ij} is the modulus of the mean strain rate tensor; $A_0=4.0$ and $A_s=\sqrt{6}\cos\varphi$ are the model constants.

Solution domain, initial and boundary conditions

The conditions set for the numerical simulations were the same as the prototype engineering. The computerized analysis of the flow was undertaken using ANSYS Fluent software. A Quadratic Upstream Interpolation for Convective Kinematics (QUICK) discretization scheme was used for the momentum equation and for the turbulent closure quantities. A Pressure Implicit with Splitting of Operators (PISO) algorithm was employed for pressure-velocity coupling. At the inlet boundary, experimentally measured x-direction velocity was used as the initial velocity, and the turbulence intensity was set to 8%. The pressure of the upper boundary and the outlet is standard atmospheric pressure. A no-slip boundary condition was applied by specifying the velocity components to be zero at the fluid-wall

interface. The viscous sub-layer is addressed using a standard wall function.

The geometry of the 3D solution domain and the boundary conditions used for the numerical simulations are shown in Figure 2. Hybrid meshes are adopted, which consist of hexahedron cells and tetrahedral cells. There are about 0.41 million cells in total. The boundary layer meshes are generated near the wall. Table 1 shows a list of numerical simulations.

VALIDATION OF NUMERICAL MODEL

A grid convergence index (GCI) was determined (Celik *et al.* 2008; Safarzadeh & Noroozi 2016; Sajjadi *et al.* 2016) for the verification of computed velocities. Three mesh systems were used to examine the effect of mesh size on the numerical results: mesh 1 (coarser, 0.07 million cells), mesh 2 (medium, 0.15 million cells), and mesh 3 (fine, 0.41 million cells).

In this study, the centerline velocities (x-direction) at the position of 1.25 m above the floor were used to determine the numerical uncertainties due to discretization. Table 2 shows the assessment of GCI values. It is seen that the maximum discretization uncertainty of the velocities for the fine-grid solutions is 1.6%, which is an excellent indication.

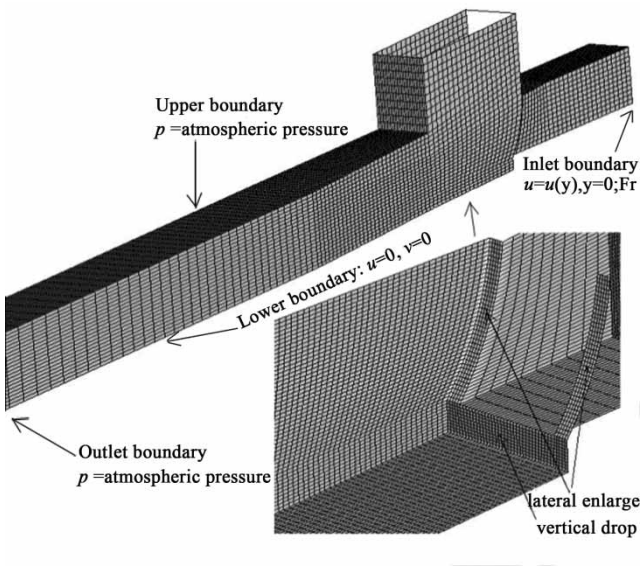

Figure 2 | Grid mesh of the numerical model.

Table 1 | Cases of the simulation

Case	Orifice opening ratio	Water head before gate(m)	Discharge(m^3/s)	Fr
1	$K = 1.0$	107.40	357.70	6.59
2	$K = 1.0$	89.65	326.00	5.77
3	$K = 0.5$	107.40	176.40	6.59
4	$K = 0.5$	89.65	160.80	5.77

RESULTS AND ANALYSIS

Water surface profiles and aeration cavity

Both the calculated water fraction (water-vof) and measured flow surface profiles (thick lines) are presented in Figure 3. It can be seen that the simulated results are in qualitative agreement and match well with the experiment's values. It is worth noting that a clear water regime (namely, a triangular zone of un-aeration) was generated downstream of the sudden fall-expansion aerator under the condition of the radial gate being half-open (Figure 3(c) and 3(d)). In addition, the morphologies of lateral cavities are shown in Figure 4. The results indicated that both the lateral and bottom cavity length are decreased with decreasing discharge in front of the gate. When the gate is half-open, the flow becomes unstable and the lateral cavity almost disappeared, obscured by the spray and mist from the curtain of water; moreover, the

Table 2 | GCI values in x-direction velocity profile ($K = 1.0$, Fr = 5.77)

(x, y, z)	V_x(m/s)	GCI_{32}^{fine}
(532.594, 0, 776.027)	20.004	0.89%
(534.144, 0, 776.005)	19.470	0.91%
(536.211, 0, 775.977)	18.995	1.26%
(538.794, 0, 775.941)	18.842	0.79%
(540.861, 0, 775.912)	19.249	1.18%
(543.961, 0, 775.869)	19.734	1.60%
(546.028, 0, 775.840)	19.828	0.31%
(549.644, 0, 775.790)	20.005	0.30%
(554.294, 0, 775.725)	20.078	0.03%
(557.394, 0, 775.682)	19.840	0.04%
(559.461, 0, 775.653)	19.987	0.01%

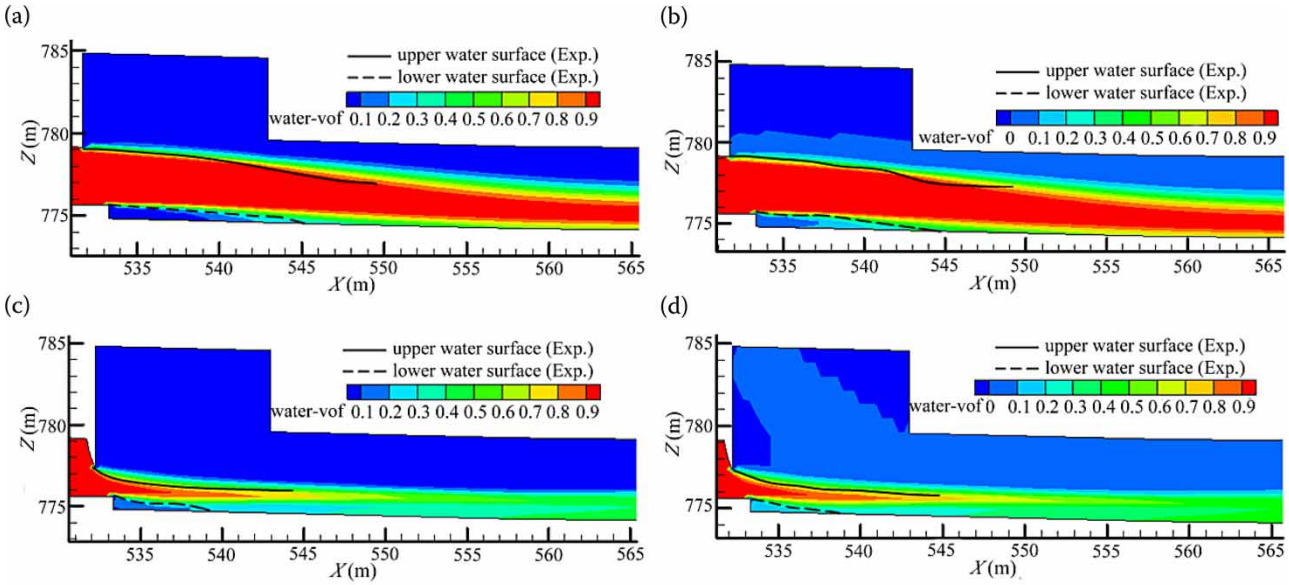

Figure 3 | Experiment and numerical results of water surface profiles: (a) case 1; (b) case 2; (c) case 3; (d) case 4.

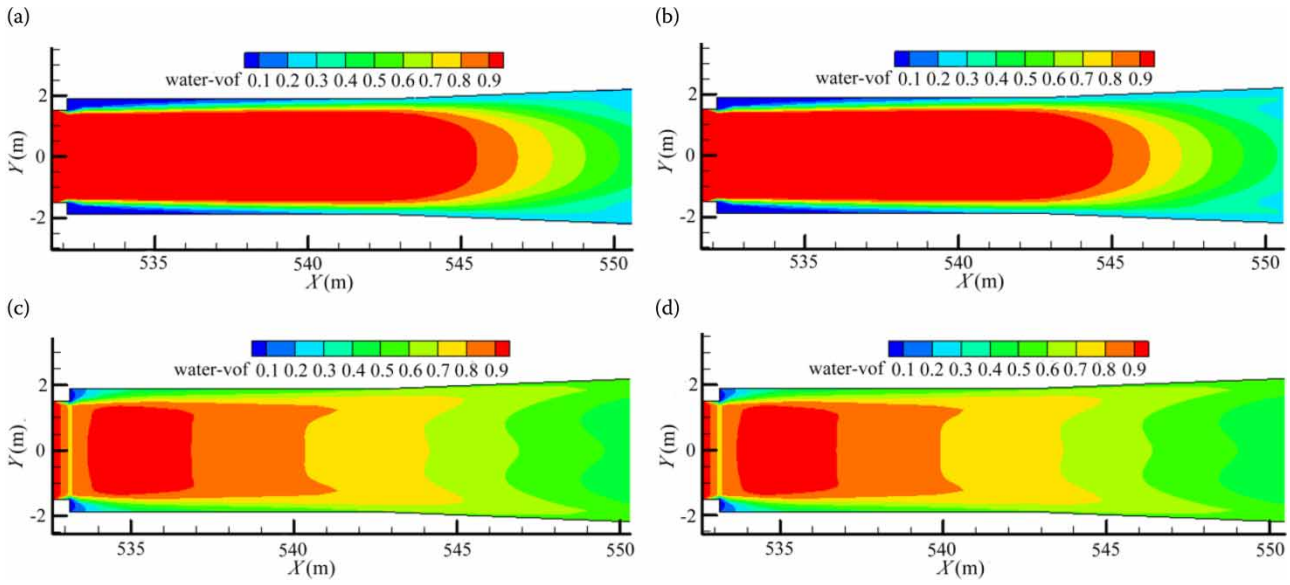

Figure 4 | The morphologies of lateral cavities: (a) case 1; (b) case 2; (c) case 3; (d) case 4.

bottom cavity length is shortened due to the filling of backwater (cases 3 and 4).

Pressure distributions

The iso-pressure curves are illustrated in Figure 5. It is evident that the flow on both the sidewalls and floor can be divided into four regimes: the cavity regime, the impact regime, the reflective regime and the stable regime. The pressure in the cavity zone is small, or even less than zero. A large pressure gradient and pulsation were generated close to the impinged point in the impact regime, where the water lashed against the sidewalls and floor. The pressure reduced significantly in the reflection zone because

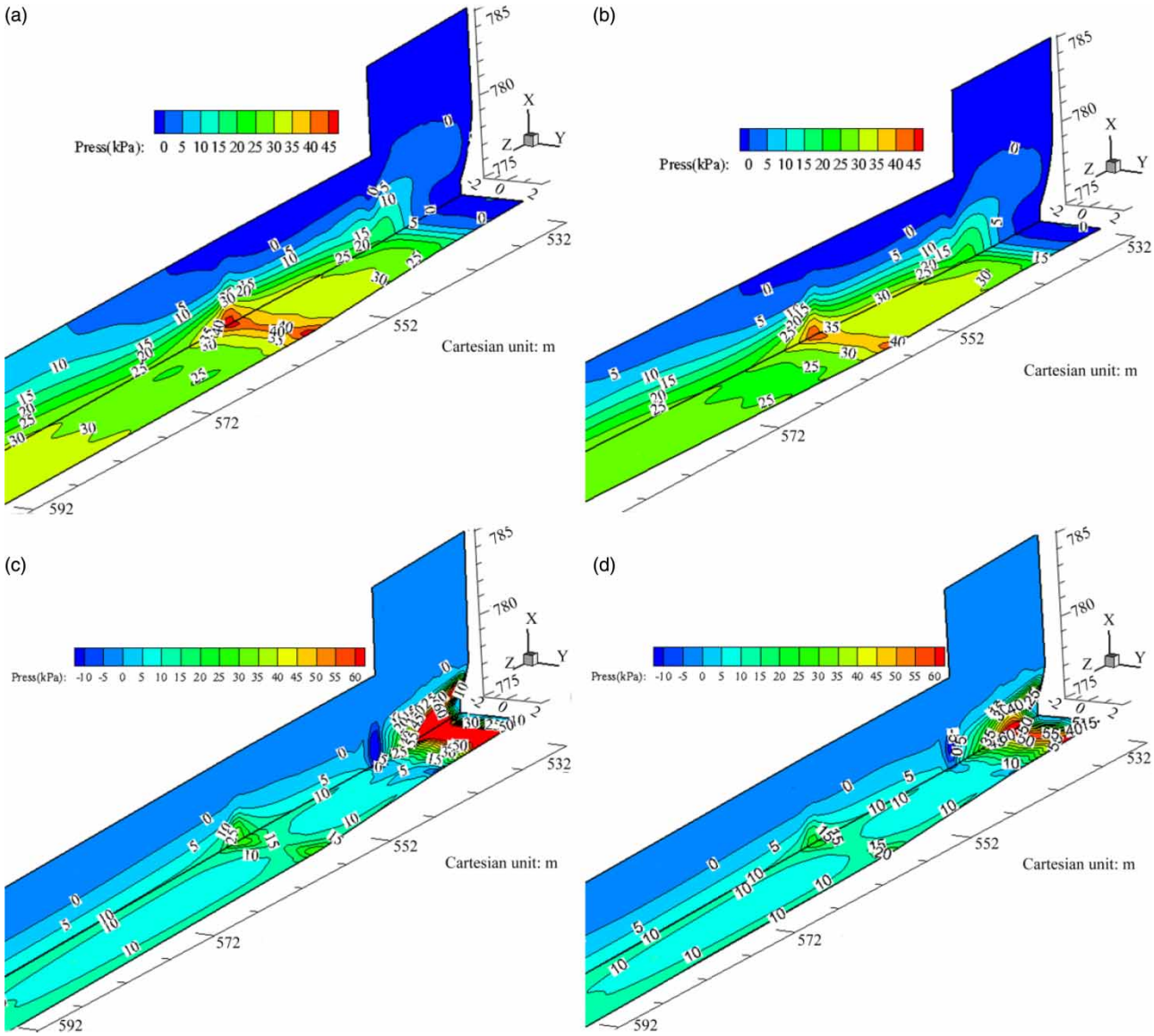

Figure 5 | The pressure distributions on both the floor and sidewall: (a) case 1; (b) case 2; (c) case 3; (d) case 4.

of the reflex action of flow, and then gradually adjusted to normal distribution in the stable zone. When the gate is fully open, the time-average pressure showed a unimodal distribution with no negative pressure. The maximum pressure in cases 1 and 2 both occurred in the impact regime. When the radial gate is half open, the time-average pressure presented a bimodal distribution. The first peak is located close to the radial gate. The position of the second peak is in the same regime as the peak when the gate is fully open. Between the two peaks, a negative pressure regime is generated near the first peak. The maximum absolutely negative pressures in cases 3 and 4 are both located in the same regime on the sidewall, where it is prone to cavitation damage due to the negative pressure, the short cavity length and insufficient air concentration.

The numerical results of iso-pressure curves and water fraction (water-vof) on the sidewall of cases 3 and 4 are shown in Figure 6. The negative pressure regime presented an elliptic shape, and the minimum negative pressure is located at the center. The range of negative pressure

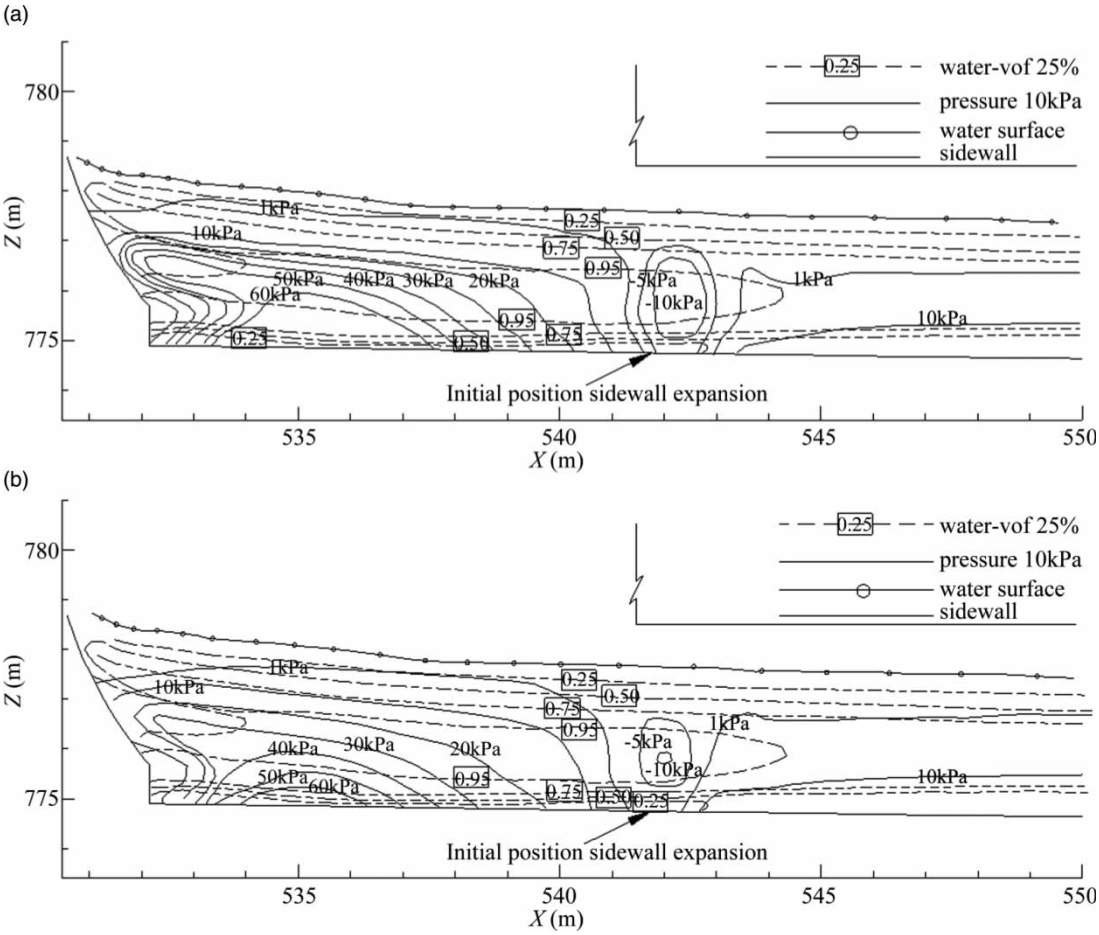

Figure 6 | The pressure contour-line and water-vof along the sidewall: (a) case 3; (b) case 4.

expanded along the upstream and downstream directions with increasing flow discharge, but the center of the negative pressure regime is basically stable.

Cavitation characteristic

Cavitation occurred when the pressure was lower than the corresponding vapor pressure. The general expression for the dimensionless cavitation index σ is given by Falvey (1990) as follows:

$$\sigma = \frac{p_0 - p_v}{\rho v_0^2/2} \tag{7}$$

where p_0 is local reference pressure; p_v is water vaporization pressure under normal temperature, equivalent to 0.24 m water column under 20 °C; v_0 is the mean velocity of the cross section.

From the experimental data, the distributions of the flow cavitation index were in qualitative agreement and matched well with the numerical calculation results (Figure 7). It is evident that the flow cavitation index on the sidewall along the tunnel is less than 0.3, in particular, σ may be less than 0.2 when the gate is half open. Falvey (1990) presented a diagram based upon a series of data of damaged structures relating to time of exposure and cavitation index. It was proposed that a cavitation index of 0.20 should be considered the lower limit to avoid cavitation damage (Frizsel & Melford 1991; Rajasekhar *et al.* 2014). When the flow cavitation index is more than 0.2, the possibility of cavitation erosion on the wall is low. The high speed flow is more likely to cause cavitation damage on the sidewall of the tunnel with the radial gate partly open. The

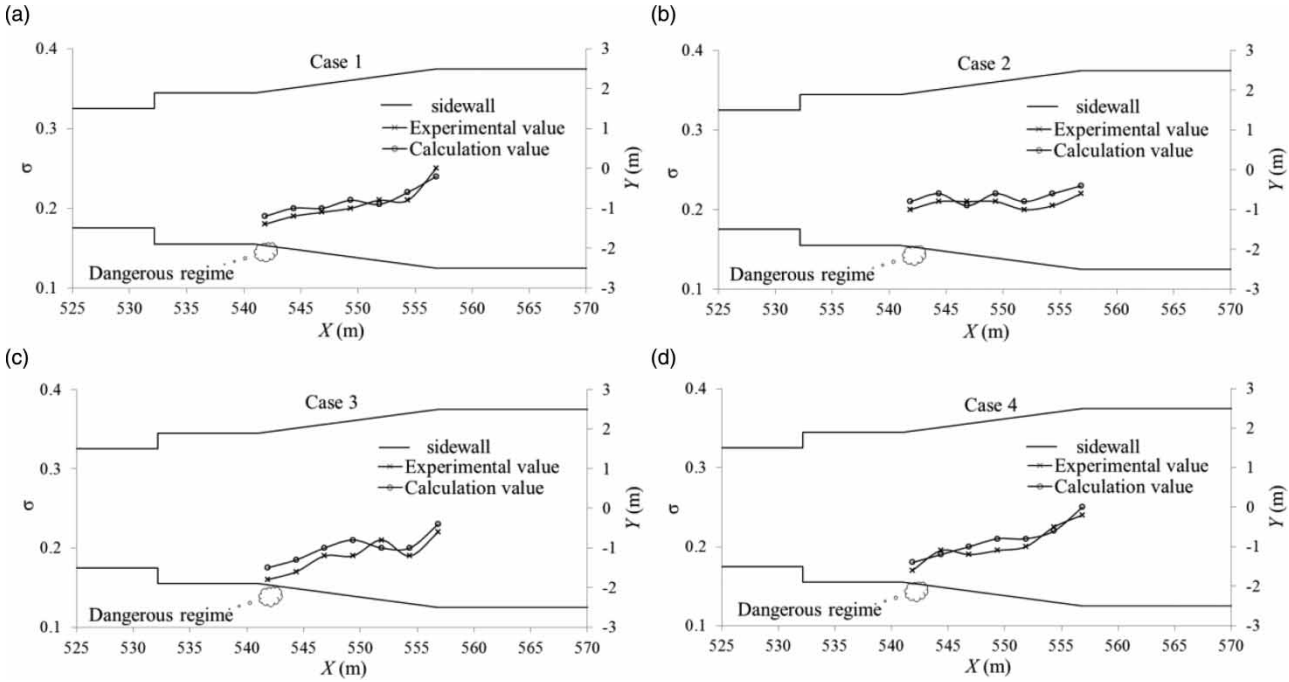

Figure 7 | The distribution of the flow cavitation index along the sidewall.

reason may be attributed to the large negative pressure, low air concentration and small cavitation index. Therefore, the hydraulic tunnel using lateral sidewall aeration should avoid the sidewall diffusion downstream of the close-wall impact zone. Meanwhile, operators should minimize running the radial gate partly open and at a low water head.

CONCLUSIONS

(1) There was good agreement between the experimental data and the numerical results for water surface profiles, pressure distributions and the flow cavitation index in the tunnel. The results substantiate that the realizable $k-\varepsilon$ turbulence model can simulate well the flow downstream of a radial gate with a sudden fall-expansion aerator in the tunnel.

(2) The flow becomes unstable and cavity length decreases sharply when the gate is partly open. The pressure distribution can be divided into four regimes: the cavity regime, the impact regime, the reflective regime and the stable regime. When the gate is fully open, the distribution of the time-average pressure is subject to a unimodal distribution, whereas the time-average pressure presented a bimodal distribution when the gate was partly open. In the middle of the two peaks, a negative pressure regime is formed and presented an elliptic shape with the minimum pressure in the center.

(3) When the gate is half open, the flow cavitation index is less than 0.2 on the sidewall downstream of the aerator, also the negative pressure regime and low air concentration all exist on the sidewall. The reason for the cavitation erosion on the sidewall can be attributed to the partly opened radial gates and the sidewall diffusion downstream of the aerator. The results can provide a reliable basis for optimizing the design of a flood discharging tunnel and gate operation.

FUNDING

This work was partly supported by the Young Science Foundation of Key Laboratory of Mountain Hazards and Earth Surface Processes, CAS (grant Y3L1340340), China Postdoctoral Science Foundation (grant 2016M602716), the

National Science Fund for Distinguished Young Scholars (grant 51625901) and the Natural Science Foundation of China (grant 51579165).

REFERENCES

Aghebatie, B. & Hosseini, K. 2016 Analyzing the turbulent flow on steep open channels. *Water Science and Technology: Water Supply* **16** (5), 1207–1213. doi:10.2166/ws.2016.043.

Arantes, E. J., Porto, R. M., Gulliver, J. S., Lima, A. & Schulz, H. E. 2010 Lower nappe aeration in smooth channels: experimental data and numerical simulation. *Anais da Academia Brasileira de Ciências* **82** (2), 521–537.

Bai, R., Zhang, F., Liu, S. & Wang, W. 2016 Air concentration and bubble characteristics downstream of a chute aerator. *International Journal of Multiphase Flow* **87**, 156–166.

Bazargan, J. & Aghebatie, B. 2015 Numerical analysis of roll waves in chutes. *Water Science and Technology: Water Supply* **15** (3), 517–524. doi:10.2166/ws.2014.136.

Celik, I. B., Ghia, U., Roache, P. J. & Freitas, C. J. 2008 Procedure for estimation and reporting of uncertainty due to discretization in CFD applications. *Journal of Fluids Engineering-Transactions, ASME* **130** (7), 078001. doi:10.1115/1.2960953.

Chen, J. G., Zhang, J. M., Xu, W. L. & Wang, Y. R. 2010 Numerical simulation of the energy dissipation characteristics in stilling basin of multi-horizontal submerged jets. *Journal of Hydrodynamics, Ser. B* **22** (5), 732–741. doi:10.1016/S1001-6058(09)60110-4.

Dong, Z. Y. & Su, P. L. 2006 Cavitation control by aeration and its compressible characteristics. *Journal of Hydrodynamics, Ser. B* **18** (4), 499–504. doi:10.1016/S1001-6058(06)60126-1.

Dong, Z. Y., Lei, C. & Ju, W. J. 2007 Cavitation characteristics of high velocity flow with and without aeration on the order of 50 m/s. *Journal of Hydrodynamics, Ser. B* **19** (4), 429–433. doi:10.1016/S1001-6058(07)60136-X.

Falvey, H. T. 1990 *Cavitation in Chutes and Spillways.* US Department of the Interior, Bureau of Reclamation, Denver.

Frizsel, K. H. & Melford, B. W. 1991 Designing spillways to prevent cavitation damage. *Concrete International* **13** (5), 58–64.

Hager, W. H. & Boes, R. M. 2014 Hydraulic structures: a positive outlook into the future. *Journal of Hydraulic Research* **52**, 299–310. doi:10.1080/00221686.2014.923050.

Heller, V. 2011 Scale effects in physical hydraulic engineering models. *Journal of Hydraulic Research* **49** (3), 293–306. doi:10.1080/00221686.2011.578914.

Li, G. J., Dai, G. Q., Qing, Y. & Ma, X. D. 2011 Detached eddy simulation of hydraulic characteristics along the side-wall after a new arrangement-scheme of the sudden lateral enlargement and the vertical drop. *J. Hydrodyn Ser. B* **23** (5), 669–675. doi: 10.1016/S1001-6058(10)60163-1.

Li, S., Zhang, J. M., Xu, W. L., Chen, J. G., Peng, Y., Li, J. N. & He, X. L. 2016a Simulation and experiments of aerated flow in curve-connective tunnel with high head and large discharge. *International Journal of Civil Engineering* **14** (1), 23–33. doi:10.1007/s40999-016-0012-7.

Li, S., Zhang, J. M., Xu, W. L., Chen, J. G. & Peng, Y. 2016b Evolution of pressure and cavitation on side walls affected by lateral divergence angle and opening of radial gate. *Journal of Hydraulic Engineering, ASCE* **142** (7), 05016003. doi:10.1061/(ASCE)HY.1943-7900.0001129.

Nie, M. X., Duan, B. & Li, L. L. 2006 Hydraulic characteristics along the sidewall of a sluice downstream of a sudden lateral enlargement and vertical drop. *Journal of Tsinghua University (Sci. & Tech.)* **46** (12), 1969–1972 (in Chinese).

Pfister, M. & Hager, W. H. 2010 Chute aerators. II: hydraulic design. *Journal of Hydraulic Engineering, ASCE* **136** (6), 360–367. doi:10.1061/(ASCE)HY.1943-7900.0000201.

Pfister, M., Lucas, J. & Hager, W. H. 2001 Chute aerators: Pre aerated approach flow. *Journal of Hydraulic Engineering, ASCE* **137** (11), 1452–1461. doi:10.1061/(ASCE)HY.1943-7900.0000417.

Rajasekhar, P., Santhosh, Y. V. G. & Soma, S. S. 2014 Physical and numerical model studies on cavitation phenomenon: a study on Nagarjuna Sagar Spillway. *International Journal of Recent Developments in Engineering and Technology* **2** (1), 1–10.

Safarzadeh, A. & Noroozi, B. 2016 3D hydrodynamics of trapezoidal piano key spillways. *International Journal of Civil Engineering* doi:10.1007/s40999-016-0100-8.

Sajjadi, S. A. H., Sajjadi, S. H. & Sarkardeh, H. 2016 Accuracy of numerical simulation in asymmetric compound channels. *International Journal of Civil Engineering*.doi:10.1007/s40999-016-0113-3.

Shih, T. H., Liou, W. W. & Shabbir, A. 1995 A new k-e eddy-viscosity model for high Reynolds number turbulent flows-model development and validation. *Computers and Fluids* **24** (3), 227–238.

Wu, J. & Ma, F. 2013 Cavity flow regime for spillway aerators. *Science in China Series E: Technological Sciences* **56** (4), 818–823. doi:10.1007/s11431-013-5145-1.

Zhang, J. M., Xu, W. L., Wang, W. & Liu, S. J. 2010 Cavitation damage to sidewalls in a sand flushing tunnel under high head. *J. Hydroelectr. Eng.* **29** (5), 197–201 (in Chinese).

First received 22 March 2017; accepted in revised form 10 July 2017. Available online 25 July 2017